Emergent Gauge Fields from Curvature in Single Layers of Transition-Metal Dichalcogenides

Héctor Ochoa, Ricardo Zarzuela, and Yaroslav Tserkovnyak

Phys. Rev. Lett. **118**, 026801 — Published 9 January 2017

DOI: 10.1103/PhysRevLett.118.026801

Emergent gauge fields from curvature in single layers of transition metal dichalcogenides

Héctor Ochoa, Ricardo Zarzuela, and Yaroslav Tserkovnyak
Department of Physics and Astronomy, University of California, Los Angeles, California 90095, USA

We analyze the dynamics of electrons in corrugated layers of transition metal dichalcogenides. The intrinsic (Gaussian) curvature along with the strong spin-orbit interaction leads to an emergent gauge field associated with the Berry connection of the spinor wave function. We study in detail the effect of topological defects of the lattice, namely tetragonal/octogonal disclinations and edge dislocations. Ripples and topological disorder induce the same dephasing effects as a random magnetic field, suppressing the weak localization effects. This geometric magnetic field can be detected in a Aharonov-Bohm interferometry experiment by measuring the local density of states in the vicinity of corrugations.

Introduction. Graphene and other two-dimensional crystals have served as new platforms for the controlled interplay between mechanical and electronic properties in material science.[1] Mechanical distortions are usually incorporated as a background geometry in the effective theory describing the long-wavelength dynamics of electrons.[2] In the particular case of graphene, gauge-like fields emerge due to the effect of mechanical tensions,[3] corrugations,[4] or topological defects[5] on the lattice. These fields arise as a manifestation of the chirality of the Bloch wave functions around the two inequivalent corners of the hexagonal Brillouin zone, $\mathbf{K}_{\pm}$. Single-layers of transition metal dichalcogenides[6] (TMDCs) combine these features with the strong spin-orbit coupling provided by the transition metal atoms. The latter removes the spin degeneracy of the bands due to the lack of a center of inversion in the unit cell, while preserving the spin quantum number along the out-of-plane direction because of its mirror symmetry.[7] This observation has been exploited in different proposals for spintronics and optoelectronics applications.[8] In particular, the application of tensions with trigonal symmetry leads to the formation of pseudo-Landau levels and the possibility of a quantum spin Hall effect,[9] similarly to the original proposal in bulk zinc-blende semiconductors.[10]

Accumulation of Berry phases[11] in real space yields an additional source of gauge fields. For instance, in corrugated graphene, where the spin-orbit interaction is negligible, these Berry phase effects are induced by the motion of the atomic orbital basis along with the distorted lattice.[12] This contribution, however, is purely dynamical and parametrically small at low frequencies in comparison to the aforementioned pseudo-gauge fields. In the case of TMDCs the situation may reverse: first of all, the chirality is not longer a good quantum number, so its effects are strongly attenuated for carriers close to the band edges due to the sizable gap in the band structure; second and more importantly, in the presence of corrugations the large spin-orbit coupling rotates the wave function in the spinor basis, which may engender a gauge field. We demonstrate that this is the case in this Letter: starting from a minimal Hamiltonian for the hexagonal (2H phase) crystal that incorporates the effect of curvature in the dynamics of low-energy excitations, we derive the emergence of a U(1) gauge field related to the spin-Berry connection of the wave function. The associated magnetic field is intrinsically determined by the geometry of the distorted lattice. Experimental consequences are discussed with emphasis on topological defects, which have been observed by transmission electron microscopy.[13] Our theory falls within a broader framework of interplay between topology and orientational (spin or nematic) order, with examples in nanomagnetism,[14] liquid crystals,[15] or more recently in Weyl semimetals.[16]

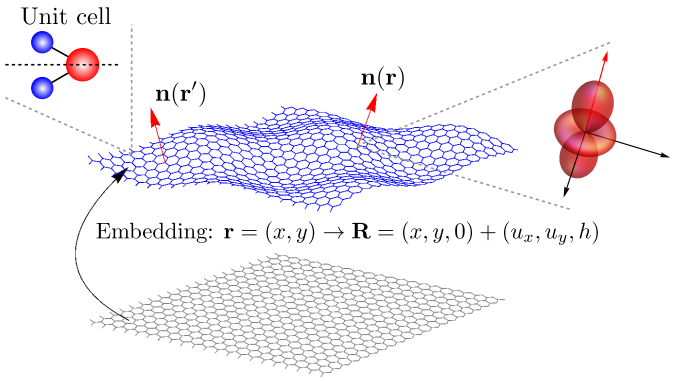

FIG. 1: Corrugated TMDC crystal in the 2H phase described as a membrane in the Monge's representation. Red arrows represent normal vectors to the surface. The unit cell consists of one transition metal and two chalcogen atoms. The dashed line represents the plane of mirror reflection. The lowest energy bands are dominated by d orbitals from the transition metal atoms. The local orbital basis (in the figure, a d_{z^2} orbital dominating the conduction band) is oriented along the normals.

Model. We are interested in the effective low-energy description of electrons in a corrugated TMDC with account of spin-orbit interactions. The $\mathbf{k}\cdot\mathbf{p}$ Hamiltonian around the two inequivalent valleys reads[7,17]

$$\mathcal{H} = \frac{\hbar^2 \boldsymbol{k}^2}{2m^*} \pm \Delta_{\rm so}\, \boldsymbol{s}\cdot\boldsymbol{n}(\boldsymbol{r}), \tag{1}$$

where $\boldsymbol{k} = -i\boldsymbol{\partial}$ is the momentum operator around the

$\mathbf{K}_\pm$ points and m^* is the effective mass of carriers near the edges of the lowest energy bands. The last term accounts for the spin-orbit coupling, where $\boldsymbol{s}$ is the vector of Pauli matrices associated with the spin degree of freedom, the $\pm$ sign applies to $\mathbf{K}_\pm$ valleys, and $\boldsymbol{n}(\boldsymbol{r})$ represents the normal to the crystal surface. Here $\boldsymbol{r} = (x, y)$ are the positions of the unit cells in the crystalline configuration, which parametrizes the surface in the so-called Monge's representation, see Fig. 1.

The Hamiltonian in Eq. (1) is expressed in an internal frame of reference, in which the local orbital basis is rotated with respect to an inertial (laboratory) frame, as depicted in Fig. 1. In the pristine crystalline phase, $\boldsymbol{n}(\boldsymbol{r}) \equiv \hat{e}_z$, the Hamiltonian is compatible with the $D_{3h} = D_3 \times \sigma_h$ point group symmetry of the lattice. Real samples may however present corrugations due to either the interaction with a substrate or thermal fluctuations, breaking the σ_h (mirror $z \to -z$) symmetry. As bands of opposite parity with respect to mirror reflection are well separated in energy, orbital hybridization can be safely neglected.[18] The mirror-symmetry breaking is then incorporated by locking the quantization axis to the normal, as imposed by the spin-orbit interaction. A similar approach has been taken in carbon nanotubes.[19] In this Letter we focus on the static case, so that $\boldsymbol{n}(\boldsymbol{r})$ depends only on spatial coordinates.

Adiabatic limit. It is convenient to study the model in the spinor basis adjusted to the local quantization axis defined by $\boldsymbol{n}(\boldsymbol{r})$. For this purpose, let us consider a local unitary rotation satisfying[20]

$$\mathcal{U}^\dagger(\boldsymbol{r})[\boldsymbol{s}\cdot\boldsymbol{n}(\boldsymbol{r})]\mathcal{U}(\boldsymbol{r}) = s_z. \tag{2}$$

The unitary operator $\mathcal{U}(\boldsymbol{r})$ implements a SU(2)/U(1)-gauge transformation on the spinor wave function. The transformed Hamiltonian is

$$\mathcal{U}^\dagger(\boldsymbol{r})\mathcal{H}\mathcal{U}(\boldsymbol{r}) = \frac{\hbar^2}{2m^*}\left[\boldsymbol{k} - \hat{\boldsymbol{A}}(\boldsymbol{r})\right]^2 \pm \Delta_{\rm so} s_z, \tag{3}$$

where the components of the gauge field read

$$\hat{A}_\mu(\boldsymbol{r}) \equiv i\mathcal{U}^\dagger(\boldsymbol{r})\partial_\mu\mathcal{U}(\boldsymbol{r}) = \hat{A}^{\rm aff}_\mu(\boldsymbol{r}) + A^{\rm B}_\mu(\boldsymbol{r})\, s_z. \tag{4}$$

We emphasize that $\hat{A}_\mu(\boldsymbol{r})$ splits into two different contributions: $\hat{A}^{\rm aff}_\mu(\boldsymbol{r})$ is univocally determined by the extrinsic curvature of the surface,[21] and therefore does not depend on the particular choice of $\mathcal{U}(\boldsymbol{r})$; on the contrary, $A^{\rm B}_\mu(\boldsymbol{r})$ does depend explicitly on this choice, which manifests the U(1) ambiguity of the theory.[22]

The gauge-independent (transverse) contribution comes from the affine connection defined by the corrugated surface. It accounts for the deviation of the spin polarization vector with respect to $\boldsymbol{n}$. This field can be recast in terms of the extrinsic curvature tensor (second fundamental form) as[18]

$$A^{\rm aff}_\mu(\boldsymbol{r}) = \frac{i}{4} f_{\mu\nu}(\boldsymbol{r})\,[s_z, s_\nu] \approx \frac{i}{4}\partial_\mu\partial_\nu h(\boldsymbol{r})\,[s_z, s_\nu]. \tag{5}$$

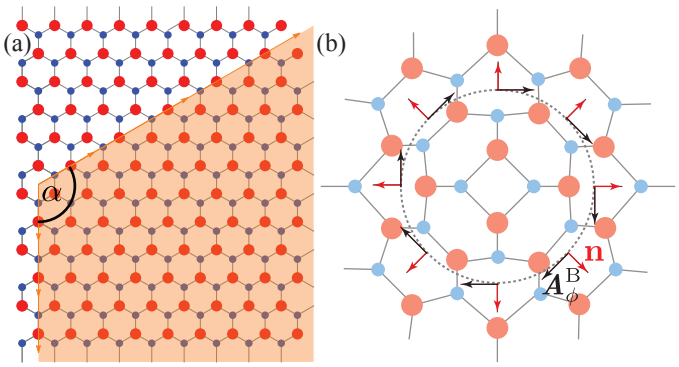

FIG. 2: (a) Tetragonal disclination in the Volterra's construction: a sector of the lattice with central angle $\alpha = \frac{2\pi}{3}$ is removed and then the boundaries are identified. (b) Top view of the resulting cone-like shape. The red arrows represent the normal to the surface, and the black ones point along the vortex field, $A^{\rm B}_\phi = -\frac{\alpha}{4\pi|\boldsymbol{r}|}$.

The last expression comes from an expansion to the lowest order in the displacement fields in the Monge's representation.

This deviation induces spin flip processes through a coupling of the form $\boldsymbol{A}^{\rm aff}(\boldsymbol{r})\cdot\boldsymbol{k}$. Due to the large spin-orbit splitting, however, spin relaxation can be neglected in the limit of smooth corrugations defined by

$$\nabla^2 h \ll \frac{\Delta_{\rm so}}{\hbar v_F}, \tag{6}$$

where v_F is the Fermi velocity of carriers. In this regime, the spin follows adiabatically the local quantization axis imposed by the spin-orbit interaction. The wave function acquires a phase while moving over a curved section of the distorted crystal, which is associated with the spin-Berry connection provided by the remaining U(1)-gauge contribution in Eq. (4). As a result, an effective magnetic field arises in the dynamics of carriers with respect to the co-moving internal frame,[18]

$$\mathcal{B}(\boldsymbol{r}) = \pm\frac{\hbar}{e}\nabla\times\boldsymbol{A}^{\rm B}(\boldsymbol{r}) = \pm\frac{\hbar}{2|e|}\kappa(\boldsymbol{r}). \tag{7}$$

Here $\kappa(\boldsymbol{r})$ is the Gaussian curvature and the sign $+(-)$ corresponds to spin up (down) electrons with respect to the local quantization axis. Notice that this is an intrinsic geometrical property of the distorted crystal.

Topological defects. The magnetic flux across the surface of the distorted crystal is quantized according to the Gauss-Bonnet theorem,[18]

$$\Phi = \int_S \mathcal{B}(\boldsymbol{r})\,{\rm d}A = \frac{\hbar}{2|e|}\int_S \kappa(\boldsymbol{r})\,{\rm d}A = \chi(S)\Phi_0. \tag{8}$$

Here $\chi(S)$ is the Euler characteristic of the corrugated surface, $\Phi_0 = h/2|e|$ is the flux quantum, and we have neglected contributions from the boundary. Any configuration smoothly connected to the flat phase has zero Euler characteristic and thus the total flux is zero. Topological defects –disclinations and dislocations– are therefore

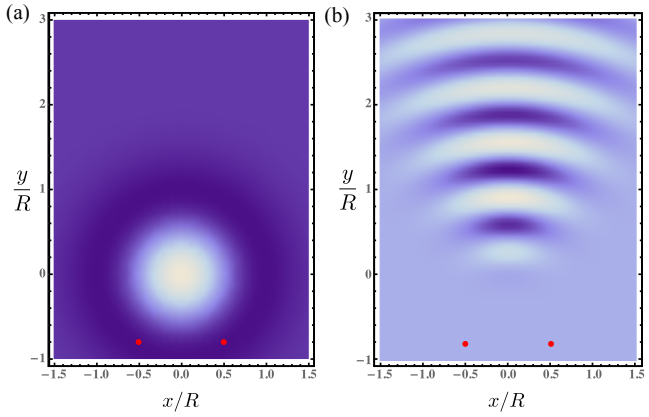

FIG. 3: (a) Magnetic field profile due to a gaussian bump, described by a heigh t profile of the form $h(\boldsymbol{r}) = h_0 e^{-|\boldsymbol{r}|^2/R^2}$. (b) Map of the local density of states at the Fermi level in arbitrary units. The model parameters are $h_0/R = 0.1$, $k_F R = 5$, $m^* U_0/2\pi\hbar^2 = 1$. The red dots represent the positions of the scattering centers.

a natural source of curvature. Isolated disclinations can be introduced into the crystal lattice via the Volterra's (cut-and-paste) construction: as depicted in Fig. 2 (a), these defects can be built by removing (adding) a sector of the lattice with central angle α –also referred to as the defect (excess) angle– and then by identifying its boundaries. This leads to a cone-like shape, see Fig. 2 (b), whose Gaussian curvature is zero everywhere except at the cusp, $\kappa(\boldsymbol{r}) = \alpha\,\delta^{(2)}(\boldsymbol{r})$.[18] Hence, we identify α with the topological charge of the defect.

In TMDC crystals, defects preserving the coordination of the lattice are the tetragonal ($\alpha_4 = \frac{2\pi}{3}$) and octogonal ($\alpha_8 = -\frac{2\pi}{3}$) disclinations. The competition between stretching and bending energies relaxes the position of the atoms. The involved strain fields are long-ranged, similarly to the case of a screw dislocation in a 3D solid.[23] The long-ranged nature of the defect is also present in the Berry-connection gauge field, which possesses the structure of a vortex, see Fig. 2 (b). The topological charge of the disclination can be understood on physical grounds as twice the Aharonov-Bohm phase acquired by the wave function when the electron surrounds the defect, a reminiscence of the removed angular sector in the Volterra's construction. With account of Eq. (8) the total spin-Berry magnetic flux reads

$$\Phi = \frac{1}{6}(n_4 - n_8)\Phi_0^{\text{Dirac}}, \tag{9}$$

where $\Phi_0^{\text{Dirac}} = h/|e|$ is the Dirac monopole flux quantum and n_4 (n_8) is the number of tetragonal (octogonal) disclinations. In asymptotically flat samples we have $n_4 = n_8$, and therefore the total flux is zero. A pair of complementary disclinations forms an edge dislocation with the Burgers vector perpendicular to the axes linking the centers of the pair. On the contrary, an imbalance in the topological charge bends the TMDC layer, eventually folding the membrane into a closed molecule. This happens when the condition $n_4 - n_8 = 6$ is met according to Euler's formula.[18] Through Eq. (9) we conclude that the topological closure is equivalent to the Dirac quantization condition, i. e. electrons experience the magnetic field created by a Dirac monopole located at the center of the molecule.

Aharonov-Bohm effect. Electrons and holes surrounding corrugated regions of the sample acquire a non-trivial phase that gives rise to quantum interference corrections to spectral properties. We propose a scanning tunnel microscopy (STM) experiment to probe the Aharonov-Bohm effect[24] on the local density of states induced by the proximity of a corrugation. Our scheme follows closely previous proposals to measure the same effect due to real[25] and pseudo-magnetic fields in graphene.[26] The simplest Aharonov-Bohm interferometer consists of two scattering centers. Processes corresponding to semiclassical closed paths between the scattering centers and the STM tip give rise to a correction in the local density of states due to the presence of curvature, $\delta\rho = \rho - \rho_{\text{flat}}$, which is evaluated as

$$\delta\rho(\boldsymbol{r},\omega) \sim -\frac{1}{\pi}\,\text{Im}\,\delta G_{\text{loop}}(\boldsymbol{r},\boldsymbol{r},\omega) \times \left[\cos\frac{\pi\Phi_{\text{loop}}}{\Phi_0} - 1\right].$$

Here $\delta G_{\text{loop}}(\boldsymbol{r},\boldsymbol{r},\omega)$ represents the correction to the local Green function due to these scattering loops, which can be computed by means of standard diagrammatic techniques.[18] In the derivation of this expression we employed the semiclassical approximation for the Green function, which is justified in the adiabatic regime, Eq. (6). The cosine factor stems from the fact that trajectories enclosing anti-clockwisely the corrugation acquire a phase proportional to the magnetic flux across the enclosed area, Φ_{loop}, whereas this phase has the opposite sign for clockwise trajectories.

We consider the case of a gaussian bump. Fig. 3 (a) shows the profile of the emergent magnetic field provided by Eq. (7). The correction to the local density of states is shown in Fig. 3 (b). The red dots represent the positions of the scattering centers. In the calculation we have assumed a scattering potential of the form $U_0\,\delta(\boldsymbol{r} - \boldsymbol{r}_i)$ and we have neglected inter-valley scattering, which is justified close to the bottom of the band.[27] Notice that the effect is not sensitive to the sign of the flux, so contributions from carriers with opposite spin sum up.

Magneto-transport. The apparent time-reversal symmetry breaking induced by corrugations and topological disorder suppresses the longitudinal magnetoconductance, $\Delta\sigma_{xx}(B) \equiv \sigma_{xx}(B) - \sigma_{xx}(0)$, in the same manner as the scattering off magnetic impurities. Related mechanisms have been previously discussed in the context of multi-valley metals.[28] The low-field magnetoconductance arises due to the partial suppression of the weak (anti-)localization correction to the conductivity. The later results from the quantum interference on self-intersecting time-reversed diffusive trajectories, along which the phase coherence of the wave function

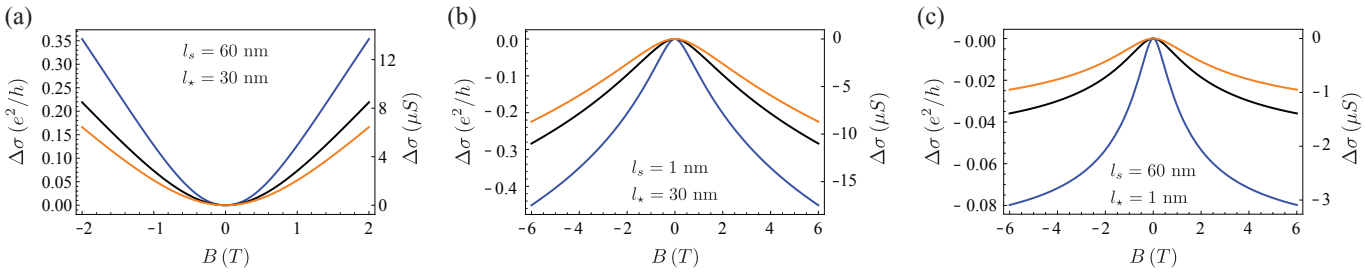

FIG. 4: Magneto-conductance of single-layer TMDCs at $T = 1.5$ K (blue), $T = 3$ K (black) and $T = 4$ K (orange) calculated via Eq (10) for the 3 regimes discussed in the text. In all cases we have considered $l_\varphi[\text{nm}] = 50/\sqrt{2.5 \times T[\text{K}]}$ in agreement with magneto-transport experiments in multi-layers.[30]

is preserved, $l_\varphi \gg \ell$. Here ℓ represents the mean free path, characterizing the typical size of diffusive loops, and l_φ is the phase coherence length limited by inelastic scattering off phonons or due to electron-electron interactions. The fictitious time-reversal symmetry breaking caused by the Gaussian curvature of the sample is only effective when the spin is conserved, $l_s \gg \ell$. Here l_s represents the spin diffusion length accounting for both inter- and intra-valley spin relaxation mechanisms. The random magnetic fields associated with the curvature of the sample define another length scale, the dephasing length $l_\star$. This irreversible dephasing mechanism opens relaxation gaps in the spin/valley mixing triplet channels of the Cooperon correlation function, leading to the magneto-conductance formula[18,29]

$$\Delta\sigma_{xx}(B) = \frac{e^2}{\pi h}\left[4F\left(\frac{B}{B_\varphi + B_s + B_\star}\right) + F\left(\frac{B}{B_\varphi + 2B_s}\right) - F\left(\frac{B}{B_\varphi}\right)\right], \tag{10}$$

where $F(x) \equiv \ln(x) + \psi\left(\frac{1}{2} + \frac{1}{x}\right)$, $\psi(x)$ is the digamma function, and $B_\alpha \equiv \hbar/4el_\alpha^2$.

Fig. 4 shows the magneto-conductance deduced from Eq. (10) for the 3 possible regimes: (a) $l_\varphi \ll l_s, l_\star$; the spin quantum number and phase coherence of the wave function are preserved along the diffusive loops responsible for the weak localization. (b) $l_s \ll l_\varphi, l_\star$; the apparent time-reversal symmetry breaking is ineffective due to spin relaxation, which engenders a phase difference $\Delta\varphi \sim \pi$ between time-reversed trajectories and therefore a destructive interference, leading to weak anti-localization and negative magneto-conductance at low fields. (c) $l_\star \ll l_s, l_\varphi$; the electrons accumulate random phases within phase coherent trajectories due to the presence of curvature, suppressing the weak (anti-)localization as time-reversal symmetry for spin up/down electrons is effectively broken. In the case of MoS_2, multi-layer samples show the usual weak localization behavior[30] characteristic of regime (a), whereas the magneto-conductance of the single-layer is 1-2 orders of magnitude lower,[31,32] compatible with regime (c). Interestingly, the negative magneto-conductance in single-layer MoS_2 reported in Ref. 32 is reproduced if we take the same inelastic coherence and spin diffusion lengths as in the multi-layer, see panel Fig. 4 (c).

Discussion. TMDC samples show similar corrugations as in graphene, with average heights of the order of $h_0 \sim 1$ nm and lateral sizes $R \sim 2 - 20$ nm.[33] The effective magnetic field at the center of these ripples is in the ballpark of $\mathcal{B} \sim \Phi_0 \left(\frac{h_0}{R^2}\right)^2 \sim 0.1 - 1$ T. Even larger fields are within experimental reach by applying compression. The large spin-orbit splittings –tens of meV in the conduction band and hundreds in the valence band– ensure the adiabatic condition for carriers close to the band edges. Interestingly, the modulation of the Fermi level leads to a crossover from the adiabatic regime, in which the gauge field stems from Berry phases in real space, to a regime dominated by pseudo-gauge fields caused by strain. This crossover should be detected in the proposed STM experiment as a variation in the interference pattern on account of the lower symmetry of the strain-induced pseudo-magnetic field, reminiscence of the structure of the wave function in reciprocal space.

We have focused on the geometric (static) aspects of the gauge theory in this Letter. Spin-dependent electromotive forces generated by dynamical membranes will be object of future research. For example, the dynamics of topological defects should pump spin analogously to the motion of solitons in magnets.[34] Reciprocally, spin currents will generate a back-action in the membrane dynamics, leading to melting instabilities due to the proliferation of topological defects. Finally, an imbalance in the number of disclinations with opposite charge will give rise to a spin-Hall response.[35]

In summary, we have shown the emergence of a gauge field associated with the spin-Berry connection in corrugated TMDC crystals. The phases accumulated by electrons and holes moving along curved sections of the crystal give rise to corrections in their single- and two-particle properties due to quantum interference. The former can be detected as a variation in the local density of states in the vicinity of corrugations and topological defects, whereas the latter may explain the suppressed localization effects observed in magneto-transport experiments in single-layer MoS_2,[31,32] in contrast to the con-

ventional weak localization behavior in the multi-layer counterpart.[30] This analysis could be extended to other systems such as zinc-blende semiconductors and surface states of topological insulators.

Acknowledgements. This work has been supported by the U.S. Department of Energy, Office of Basic Energy Sciences under Award No. DE-SC0012190 (H.O.), and by the NSF-funded MRSEC under Grant No. DMR-1420451 (R.Z.). R.Z. also thanks Fundación Ramón Areces for a postdoctoral fellowship within the XXVII Convocatoria de Becas para Ampliación de Estudios en el Extranjero en Ciencias de la Vida y de la Materia.

[1] M. A. Vozmediano, M. I. Katsnelson, and F. Guinea, Phys. Rep. **496**, 109 (2010); B. Amorim *et al.*, *ibid.* **617**, 1 (2016).
[2] Fernando de Juan, Alberto Cortijo, and María A. H. Vozmediano, Phys. Rev. B **76**, 165409 (2007); Fernando de Juan, Mauricio Sturla, and María A. H. Vozmediano, Phys. Rev. Lett. **108**, 227205 (2012).
[3] F. Guinea, M. I. Katsnelson, and A. K. Geim, Nat. Phys. **6**, 30 (2010).
[4] N. Levy, S. A. Burke, K. L. Meaker, M. Panlasigui, A. Zettl, F. Guinea, A. H. Castro Neto, and M. F. Crommie, Science **329**, 544 (2010).
[5] J. González, F. Guinea, and M. A. H. Vozmediano, Phys. Rev. Lett. **69**, 172 (1992); Nucl. Phys. B **406**, 771 (1993); Alberto Cortijo and María A. H. Vozmediano, *ibid.* **763**, 293 (2007).
[6] Q. H. Wang, K. Kalantar-Zadeh, A. Kiss, J. N. Coleman, and M.S. Strano, Nat. Nanotechnol. **7**, 699 (2012).
[7] Di Xiao, Gui-Bin Liu, Wanxiang Feng, Xiaodong Xu, and Wang Yao, Phys. Rev. Lett. **108**, 196802 (2012).
[8] Kin Fai Mak, Keliang He, Jie Shan, and Tony F. Heinz, Nat. Nanotechnol. **7**, 494 (2012); Deep Jariwala, Vinod K. Sangwan, Lincoln J. Lauhon, Tobin J. Marks, and Mark C. Hersam, ACS Nano **8**, 1102 (2014); Xiaodong Xu, Wang Yao, Di Xiao, and Tony F. Heinz, Nat. Phys. **10**, 343 (2014).
[9] M. A. Cazalilla, H. Ochoa, and F. Guinea, Phys. Rev. Lett. **113**, 077201 (2014).
[10] B. A. Bernevig and S.-C. Zhang, Phys. Rev. Lett. **96**, 106802 (2006).
[11] M. V. Berry, Proc. R. Soc. Lond. A **392**, 45 (1984).
[12] Mircea Trif, Pramey Upadhyaya, and Yaroslav Tserkovnyak, Phys. Rev. B **88**, 245423 (2013).
[13] Goki Eda, Takeshi Fujita, Hisato Yamaguchi, Damien Voiry, Mingwei Chen, and Manish Chhowalla, ACS Nano, **6**, 7311 (2012); Amin Azizi *et al.*, Nat. Commun. **5**, 4867 (2014); Thuc Hue Ly *et al.*, *ibid.* **10**, 1038 (2016).
[14] Oleksandr V. Pylypovskyi, Volodymyr P. Kravchuk, Denis D. Sheka, Denys Makarov, Oliver G. Schmidt, and Yuri Gaididei, Phys. Rev. Lett. **114**, 197204 (2015).
[15] P. de Gennes and J. Prost, *The Physics of Liquid Crystals* (Clarendon Press, Oxford, 1993).
[16] Yizhi You, Gil Young Cho, and Taylor L. Hughes, Phys. Rev. B **94**, 085102 (2016).
[17] H. Ochoa and R. Roldán, Phys. Rev. B **87**, 245421 (2013); H. Ochoa, F. Guinea, and V. I. Fal'ko, *ibid.* **88**, 195417 (2013).
[18] See Supplementary Material.
[19] Mark S. Rudner and Emmanuel I. Rashba, Phys. Rev. B **81**, 125426 (2010).
[20] N. Nagaosa, *Quantum Field Theory in Strongly Correlated Electronic Systems* (Springer, New York, 1999).
[21] Manfredo P. do Carmo, *Differential Geometry of Curves and Surfaces* (Prentice-Hall, New Jersey, 1976).
[22] $\hat{A}_\mu$ takes values in the algebra of SU(2), but the Hamiltonian in Eq. (3) exhibits only U(1) gauge symmetry. Under a local U(1) transformation of the spinor wave function, $\psi \to e^{i\zeta(\boldsymbol{r})s_z}\psi$, the components of the gauge field transform as $\hat{A}_\mu(\boldsymbol{r}) \to \hat{A}_\mu(\boldsymbol{r}) + \partial_\mu\zeta(\boldsymbol{r})s_z$.
[23] P. M. Chaikin and T. C. Lubensky, *Principles of Condensed Matter Physics* (Cambridge University Press, Cambridge, 1995).
[24] Y. Aharonov and D. Bohm, Phys. Rev. **115**, 485 (1959).
[25] A. Cano and I. Paul, Phys. Rev. B **80**, 153401 (2009).
[26] Fernando de Juan, Alberto Cortijo, María A. H. Vozmediano, and Andrés Cano, Nat. Phys. **7**, 810 (2011).
[27] Inter-valley scattering must be accompanied by spin-flip due to the spin-orbit splitting. At the band edge this process is forbidden by time-reversal symmetry. Therefore, the phase space for inter-valley scattering is very narrow when the Fermi level is close to the bottom of the band, see Tetsuro Habe and Mikito Koshino, Phys. Rev. B **93**, 075415 (2016).
[28] S. V. Iordanskii and A. E. Koshelev, JETP Lett. **41**, 574 (1985); S. V. Morozov *et al.*, Phys. Rev. Lett. **97**, 016801 (2006); E. McCann, K. Kechedzhi, V. I. Fal'ko, H. Suzuura, T. Ando, and B. L. Altshuler, Phys. Rev. Lett. **97**, 146805 (2006); A. F. Morpurgo and F. Guinea, Phys. Rev. Lett. **97**, 196804 (2006).
[29] Hector Ochoa, Francesca Finocchiaro, Francisco Guinea, and Vladimir I. Fal'ko, Phys. Rev. B **90**, 235429 (2014).
[30] Adam T. Neal, Han Liu, Jiangjiang Gu, and Peide D. Ye, ACS Nano **7**, 7077 (2013).
[31] H. Schmidt, I. Yudhistira, L. Chu, A. H. Castro Neto, B. Özyilmaz, S. Adam, and G. Eda, Phys. Rev. Lett. **116**, 046803 (2016).
[32] Davide Costanzo, Sanghyun Jo, Helmuth Berger, and Alberto F. Morpurgo, Nature Nanotechnology **11**, 339 (2016).
[33] Jacopo Brivio, Duncan T. L. Alexander, and Andras Kis, Nano Lett. **11**, 5148 (2011).
[34] Kjetil Magne, Dørheim Hals, Anh Kiet Nguyen, and Arne Brataas, Phys. Rev. Lett. **102**, 256601 (2009).
[35] Analogously to the anomalous Hall effect in ferromagnets, a dilute concentration ρ of disclinations with charge α engenders an additional term in the spin-Hall conductivity, $\sigma_{xy}^{\rm sH} \approx \frac{\hbar\tau\sigma_{xx}}{2m^*}\alpha\rho$, where $\sigma_{xx} = \frac{e^2 n\tau}{m^*}$ is the Drude conductivity, n is the carrier concentration, and τ is the scattering time.